Developmental mechanism of the periodic membrane skeleton in axons

Guisheng Zhong[1†]**, Jiang He**[2†]**, Ruobo Zhou**[1]**, Damaris Lorenzo**[3,4]**, Hazen P Babcock**[5]**, Vann Bennett**[4,6]**, Xiaowei Zhuang**[1,7]*****

[1]Department of Chemistry and Chemical Biology, Howard Hughes Medical Institute, Harvard University, Cambridge, United States; [2]Department of Molecular and Cellular Biology, Howard Hughes Medical Institute, Harvard University, Cambridge, United States; [3]Department of Biochemistry, Duke University, Durham, United States; [4]Department of Neurobiology, Duke University, Durham, United States; [5]Center for Brain Sciences, Harvard University, Cambridge, United States; [6]Department of Biochemistry, Howard Hughes Medical Institute, Duke University, Durham, United States; [7]Department of Physics, Harvard University, Cambridge, United States

Abstract Actin, spectrin, and associated molecules form a periodic sub-membrane lattice structure in axons. How this membrane skeleton is developed and why it preferentially forms in axons are unknown. Here, we studied the developmental mechanism of this lattice structure. We found that this structure emerged early during axon development and propagated from proximal regions to distal ends of axons. Components of the axon initial segment were recruited to the lattice late during development. Formation of the lattice was regulated by the local concentration of βII spectrin, which is higher in axons than in dendrites. Increasing the dendritic concentration of βII spectrin by overexpression or by knocking out ankyrin B induced the formation of the periodic structure in dendrites, demonstrating that the spectrin concentration is a key determinant in the preferential development of this structure in axons and that ankyrin B is critical for the polarized distribution of βII spectrin in neurites.
DOI: 10.7554/eLife.04581.001

*For correspondence: zhuang@
chemistry.harvard.edu

†These authors contributed
equally to this work

Introduction

Neurons are highly polarized cells with their somatodendritic regions receiving synaptic inputs and axons propagating electrical signals and sending synaptic outputs to target cells. Cytoskeletal proteins are important for maintaining the polarity of neurons. For example, actin and microtubules are essential for the growth and stabilization of axons, the trafficking of cargos to specific neurites, and the stabilization and plasticity of synapses (*Luo, 2002*; *Dent and Gertler, 2003*; *Cingolani and Goda, 2008*; *Barnes and Polleux, 2009*; *Kapitein and Hoogenraad, 2011*; *Stiess and Bradke, 2011*). Transient destabilization of actin at the tip of a neurite is sufficient to induce a dendrite to become an axon (*Bradke and Dotti, 1999*). Increasing evidence also suggests an important role for spectrin in the maintenance of neuronal polarization, as well as the development and stabilization of axons (*Hammarlund et al., 2007*; *Galiano et al., 2012*). αII and βII spectrin are enriched in axons (*Riederer et al., 1986*; *Galiano et al., 2012*). Spectrin is known to be important for providing the mechanical stability for axons (*Hammarlund et al., 2007*) and protecting them from mechanical stress (*Krieg et al., 2014*), for axon path finding (*Hulsmeier et al., 2007*), for the stabilization of pre-synaptic terminals (*Pielage et al., 2005*), and for maintaining specific membrane domains in axons (*Susuki and Rasband, 2008*). Mice lacking either αII or βII spectrin die in the embryo, highlighting the crucial function of these proteins (*Tang et al., 2003*; *Stankewich et al., 2011*; *Galiano et al., 2012*). Spectrin has also been shown to play a role in human neurological diseases (*Ikeda et al., 2006*; *Writzl et al., 2012*).

eLife digest The brain contains hundred types of neurons, but they are all variations on the same basic structure. Each neuron consists of a cell body that is covered in short protrusions called dendrites and a long thin structure called the axon. The dendrites receive incoming signals from neighboring neurons and they transmit these signals via the cell body to the axon, which in turn relays them to the dendrites of the next neuron (or neurons).

Like all cells, neurons maintain their structure with the help of an internal cytoskeleton made up of many different proteins. However, it was discovered recently that axons have an additional lattice-like structure underneath their outer membrane. This structure, which consists of rings of actin filaments separated by molecules of a protein called spectrin, is preferentially formed in axons and is found much less frequently in dendrites.

Now Zhong, He et al., who are members of the research group that discovered the axonal skeleton, have used 'super-resolution imaging' to figure out how this skeleton forms and why it predominantly forms in axons. In brief, a basic version of the sub-membrane periodic skeleton is laid down early in development, starting next to the cell body before gradually spreading down the axon. The skeleton then continues to mature throughout development with the incorporation of several additional types of proteins.

The periodic skeleton only forms in regions which contain enough βII spectrin. Under normal conditions, dendrites contain too little βII spectrin to support the growth of such a periodic skeleton. However, artificially increasing the amount of βII spectrin present by overexpressing the corresponding gene, or by knocking out ankyrin B (a molecule that is important for establishing the preferential distribution of βII spectrin in axons), is sufficient to trigger periodic skeleton formation in dendrites. Given that axons and dendrites have distinct roles in neuronal signaling, this uneven distribution of spectrin is likely to be one way in which these regions maintain the specific structures that support their individual functions.

Recently, we discovered a periodic sub-membrane lattice structure made of actin, spectrin, and other associated molecules in the axons of mammalian neurons (*Xu et al., 2013*). In this membrane skeleton, actin filaments form a ring-like structure that wraps around the circumference of axons. These actin rings are evenly spaced along the axon shaft with a period of ~190 nm and show a remarkably long-range order. Actin filaments in the rings are capped by adducin. Adjacent actin rings are connected by spectrin, likely in the form of αII-βII-spectrin heterotetramers, given the observations that the periodic βII spectrin rings alternate with the actin–adducin rings along axons and that the observed 190 nm period matches the length of the spectrin tetramer. The ultrastructural organization of this quasi-one-dimensional, periodic lattice structure is different from the previously observed, two-dimensional polygonal membrane skeletal structure found in red blood cells (*Byers and Branton, 1985*; *Liu et al., 1987*; *Bennett and Lorenzo, 2013*), whereas an erythrocyte-like polygonal membrane skeletal was observed in the axon terminals at the *Drosophila* neuromuscular junction (*Pielage et al., 2008*). Interestingly, this periodic structure preferentially forms in axons, with the actin in dendrites primarily adopting the form of long filaments running along the dendrite shaft (*Xu et al., 2013*). In *Caenorhabditis elegans* that lack β spectrin or carry a β spectrin mutant, axons break more easily during animal movement (*Hammarlund et al., 2007*) and exhibit impaired touch sensation (*Krieg et al., 2014*), suggesting that this structure may be important for the mechanical stability of axons and for sensing mechanical stimuli. This periodic lattice also organizes the axonal membrane by placing important membrane proteins, such as the voltage-gated sodium channels, into a periodic distribution (*Xu et al., 2013*).

However, it is unknown how this highly regular membrane skeleton structure develops in axons and how its formation is regulated. For example, it is unclear whether the periodic lattice develops during early or late stages of axon differentiation. Although protein factors previously identified to be important for axon differentiation tend to be enriched and function at the growing tips of axons (*Arimura and Kaibuchi, 2007*; *Barnes and Polleux, 2009*; *Stiess and Bradke, 2011*; *Cheng and Poo, 2012*), it is unknown whether the actin–spectrin lattice also initiates at the distal ends of axons or instead forms first in the proximal region near the cell body. Finally, the molecular mechanism that regulates the

specific formation of this periodic structure in axons, instead of dendrites, remains a mystery. In this study, we addressed these important questions concerning the development of this newly discovered neuronal structure. We found that the periodic membrane skeleton initiated early during axon differentiation. The lattice structure originated in the axonal region adjacent to the cell body and propagated to the distal ends of axons. The lattice structure further matured by recruiting other components, and the matured membrane skeleton was highly stable. Multiple molecular factors played roles in regulating the formation of this structure. The lattice structure depended on intact microtubules. The high local concentration of βII spectrin in axons was the key determining factor for the specific formation of the lattice structure in axons, and artificially increasing the concentration of βII spectrin in dendrites was sufficient to induce the formation of the periodic lattice structure in dendrites. Remarkably ankyrin B was important for the polarized distribution of βII spectrin in neurites; in ankyrin B knockout mice, βII spectrin was evenly distributed in axons and dendrites, giving rise to a highly regular, periodic membrane skeleton in both dendrites and axons.

Results

Early development and propagation of the periodic lattice structure in axons

Neurons exhibit distinct developmental stages with different morphological characteristics during polarization (*Dotti et al., 1988*; *Arimura and Kaibuchi, 2007*; *Barnes and Polleux, 2009*; *Cheng and Poo, 2012*). In dissociated hippocampal neuronal culture, neurons first display intense lamellipodial protrusive activity in stage 1, which then leads to the emergence of multiple immature neurites in stage 2 (~1 Day in Vitro [DIV]). In stage 3 (DIV 2–4), one of these neurites breaks the symmetry and extends rapidly to become an axon. The other neurites then gradually acquire dendritic properties in stage 4 (DIV 4–7). In stage 5 (>DIV 7), neurons continue to mature and form axon initial segments, dendritic spines, and synapses. In order to determine the developmental course of the periodic membrane skeletal structure, we fixed dissociated neurons at different developmental stages, immunostained for βII spectrin, and imaged using stochastic optical reconstruction microscopy (STORM), a super-resolution imaging method that relies on switching and localizing single molecules to acquire sub-diffraction limit images (*Betzig et al., 2006*; *Hess et al., 2006*; *Rust et al., 2006*; *Huang et al., 2008*).

To illustrate how we systematically imaged and quantified this periodic structure in axons, we first imaged a neuron at DIV 10. Consistent with our previous findings (*Xu et al., 2013*), βII spectrin adopted a highly regular, periodic pattern in all regions of the axonal shaft (*Figure 1—figure supplements 1, 2*). Both Fourier transform and autocorrelation analyses showed that the βII spectrin adopted a periodic distribution with a period of ~190 nm (*Figure 1—figure supplement 1*). Similarly, actin filaments exhibited a highly periodic distribution along axon shafts (*Figure 1—figure supplement 3*). Depolymerizing the actin filaments with latrunculin A (LatA) disrupted the periodic distribution of βII spectrin (*Figure 1—figure supplement 2*), and knocking-down βII spectrin using shRNA led to a loss of the periodic actin distribution (*Figure 1—figure supplement 3*). These results indicate that the periodic organizations of actin and spectrin are interdependent, consistent with the model that adjacent actin rings are connected by the spectrin tetramers.

Next, we quantified the distribution of βII spectrin at earlier developmental stages in DIV 2, 4, and 6 neurons (*Figure 1*). *Figure 1A* shows a typical stage 3 neuron at DIV 2, with one neurite outgrowing the others and becoming an axon. Interestingly, the periodic pattern of βII spectrin has already formed in the proximal region of this axon near the cell body, as shown by both Fourier transform and autocorrelation analyses of the STORM image (*Figure 1A,C*). However, the periodic distribution did not extend far—the middle and distal parts of the same axon did not exhibit the periodic pattern (*Figure 1A,C*). Similar results were observed for other stage 3 neurons that we imaged. As neurons continued to mature, the periodic βII spectrin distribution extended to more distal regions of axons. By DIV 6, the periodic βII spectrin distribution extended for nearly the entire length of the axon, except for the very distal region (*Figure 1B,D*). Using the autocorrelation amplitude at the first peak (~190 nm) to quantify the degree of periodicity for the βII spectrin distributions, we found that the periodicity degraded quickly along axons in DIV 2 neurons but gradually extended to the distal end of the axon in later developmental stages until the structure eventually occupied nearly the entire axon (*Figure 1E* and *Figure 1—figure supplement 4*). Taken together, these results demonstrate that the
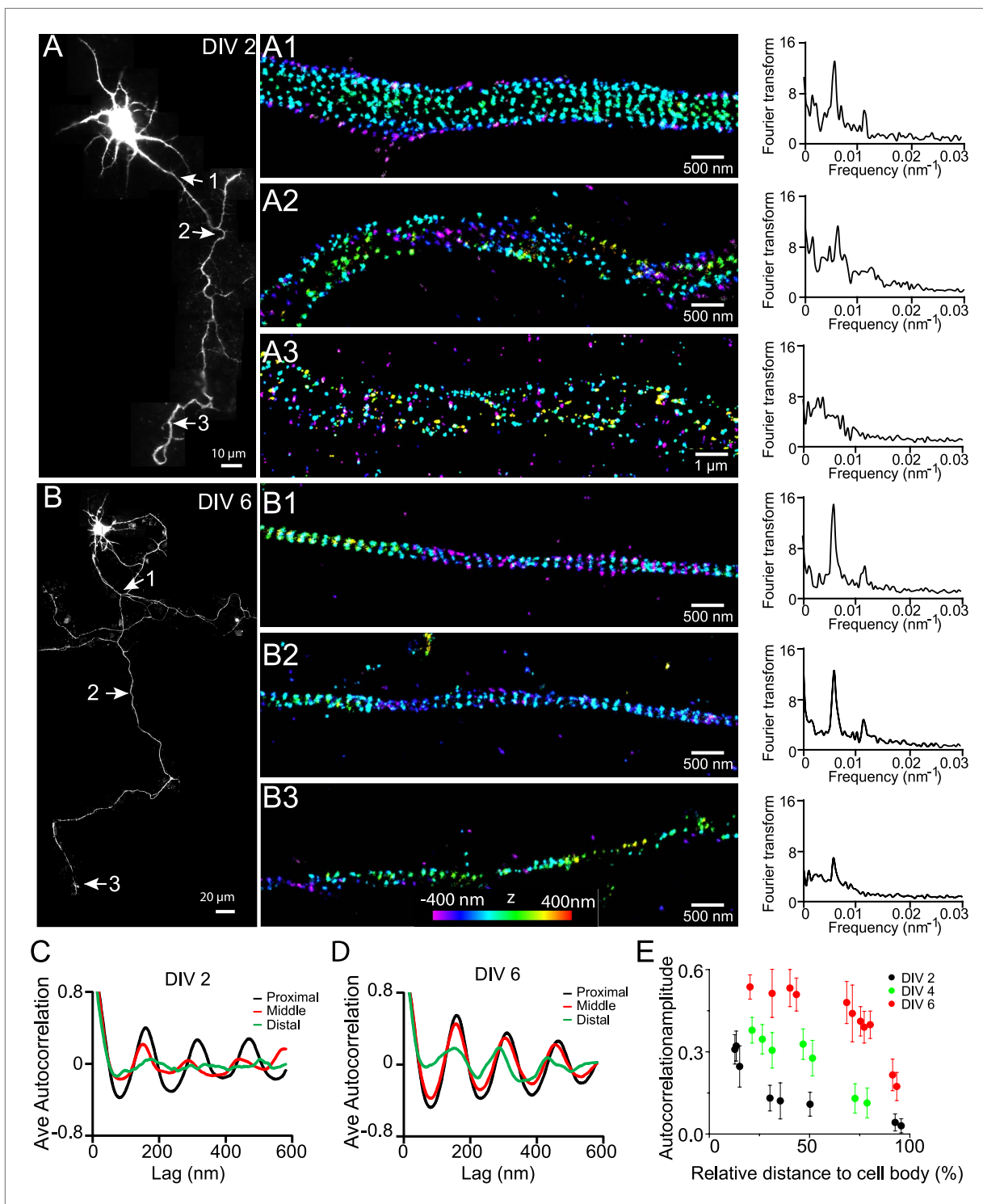
Figure 1. Early development and propagation of the periodic lattice structure in axons. (**A**) A DIV 2 neuron was stained with βII spectrin antibody and imaged by 3D STORM. The single long process from the cell is the axon. A1, A2, and A3 are 3D STORM images taken from arrow-indicated regions from **A**. The Fourier transform analyses of the βII spectrin distribution along the axon shaft are shown on the right. (**B**) Similar to (**A**), but for a DIV 6 neuron. (**C–D**) Autocorrelation analysis of βII spectrin distributions of DIV 2 (**C**) or DIV 6 (**D**) neurons at the proximal, middle, and distal regions of axons. Shown are the averaged autocorrelation from multiple segments of axons for each condition. (**E**) The average amplitude of autocorrelation analysis for different axonal regions of DIV 2, 4, and 6 neurons. The amplitude was measured as the difference between the first peak and the average of the two first valleys of the autocorrelation curve. Error bars are standard deviation from measurements of multiple neurons (n = 7 neurons for DIV 2; n = 6 neurons for DIV 4;
Figure 1. Continued on next page

Figure 1. Continued

n = 9 neurons for DIV 6; from three independent experiments at each DIV). The color bar for 3D STORM image indicates the z-depth of the image and is the same for all of our STORM images.

The following figure supplements are available for figure 1:

Figure supplement 1. βII spectrin structure in a DIV 10 neuron.

Figure supplement 2. The periodic distribution of βII spectrin depends on actin.

Figure supplement 3. The periodic distribution of actin depends on βII spectrin.

Figure supplement 4. The autocorrelation analysis is not sensitive to the number of localizations present in the periodic structure within the range of the localization numbers that we detected in axon segments.

Figure supplement 5. Distributions of dendritic βII and βIII spectrin.

Figure supplement 6. The periodic actin structure is disrupted if the neurons are subjected to membrane extraction prior to fixation.

periodic membrane skeleton forms early during development, originates in proximal axon regions close to the cell body, and propagates toward the distal end of the axon.

The periodic structure was only observed in axons, but not in dendrites, during early developmental stages, whereas isolated patches of periodic βII spectrin patterns were observed in dendrites during later developmental stages (*Figure 1—figure supplement 5A–E*). However, unlike in axons, these patches did not form a cohesive lattice structure with a long-range order. Quantitatively, the average autocorrelation analysis showed much smaller amplitudes in dendrites than those in axons (*Figure 1—figure supplement 5G*), indicating a much poorer regularity of the structure in dendrites. Similar results were observed for βIII spectrin (*Figure 1—figure supplement 5F,H*), an isoform of β spectrin that is enriched in dendrites instead of axons (*Sakaguchi et al., 1998*; *Stankewich et al., 1998*; *Gao et al., 2011*).

Actin dependence during the early developmental phase of the periodic membrane skeleton

Similar to the lattice structure in mature axons, the periodic pattern of βII spectrin depended on actin during early development. Treatment of neurons with actin-depolymerizing drugs, cytochalasin D (CytoD), or LatA disrupted the periodicity of βII spectrin in DIV 3 neurons (*Figure 2A–E*). The effect of actin-depolymerizing drugs set in quickly with the periodic βII spectrin distribution substantially disrupted after several minutes of LatA treatment (*Figure 2F,G*), consistent with the drug acting directly on the lattice structure. These results indicate that actin is involved in the lattice structure during early neuronal development. The form of actin, however, appeared to be different during the early developmental stages as compared to that in mature axons. We have previously shown that the periodic pattern of actin was not directly observed in the STORM images during DIV 1–4. In DIV 5, the periodic actin pattern begins to appear in some neurons and become robustly observed in neurons at DIV 7 (*Xu et al., 2013*). Similar results were observed here (data not shown). One possible interpretation is that actin existed in a less stable form during the early developmental stages and was not preserved by our sample treatment (fixation and extraction) prior to imaging. Consistent with the notion that actin filaments in the lattice structure were less stable during early developmental stages, the periodic structure of βII spectrin was more quickly disrupted by LatA treatment during early development than in older neurons (*Figure 2G*).

We also observed a relatively slow developmental time course for the periodic pattern of adducin, an actin-capping protein (*Kuhlman et al., 1996*). The periodic pattern of adducin was not observed in axons at DIV 2 or DIV 4 (*Figure 3*). A periodic pattern began to appear at ~DIV 6 and became obvious after DIV 7 (*Figure 3* and *Figure 3—figure supplement 1*). The lack of adducin capping may have contributed to the lower stability of actin during early development stages, although it is also possible that the lower stability of actin during the early development stages made it difficult to maintain
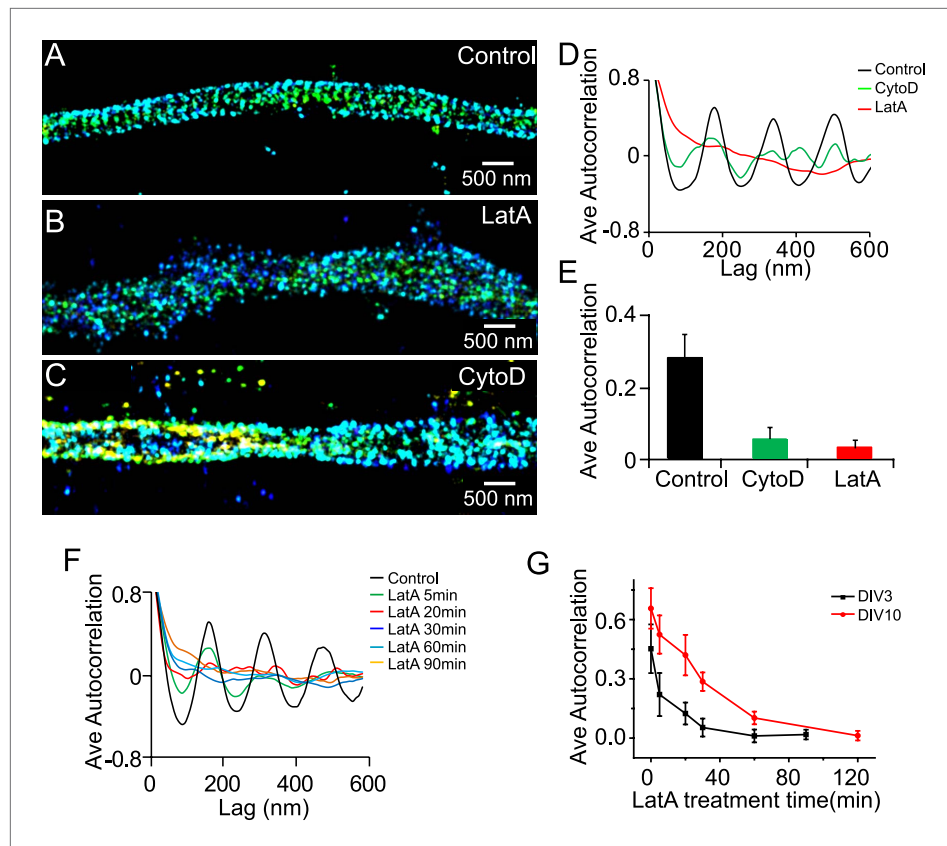
Figure 2. The periodic structure of βII spectrin depends on actin during early development. (**A–C**) DIV 3 neurons were either untreated or treated with latrunculin A (LatA, 20 μM) or cytochalasin D (CytoD, 50 μM) for 1 hr and subsequently immunostained with βII spectrin antibody for 3D STORM imaging. Shown here are representative images of βII spectrin in proximal axonal regions from control (**A**), LatA-treated (**B**) and CytoD-treated (**C**) neurons. (**D**) Average autocorrelation analyses of βII spectrin from multiple axon segments of control, LatA-treated, and CytoD-treated DIV 3 neurons (n = 6 neurons for control; n = 7 neurons for LatA-treated; n = 7 neurons for CytoD-treated conditions; at least three independent experiments for each condition). (**E**) The average autocorrelation amplitudes from control, LatA-treated, and CytoD-treated DIV 3 neurons. (**F**) Average autocorrelation analyses of βII spectrin from multiple axon segments of control and LatA-treated DIV 3 neurons at different treatment time (n > 5 neurons for each condition, three independent experiments). The axon segments are taken from the proximal axonal regions near the cell bodies. (**G**) DIV 3 and DIV 10 neurons were treated with 20 μM LatA for indicated amount of time, and the average autocorrelation amplitude of βII spectrin from these neurons are shown. Error bars are standard deviation from measurements of multiple neurons (n = 6 neurons for DIV 3; n = 8 neurons for DIV 10; four independent experiments at each DIV).
DOI: 10.7554/eLife.04581.010

the adducin pattern during cell fixation and extraction. Finally, it is formally possible that actin and adducin are not present in the periodic lattice structure during early developmental stages. However, we consider such a scenario to be less likely as it is difficult to imagine how spectrin tetramers themselves could self-assemble into a periodic lattice structure without the help of actin to crosslink multiple spectrin tetramers.

Together, the above results indicate that the periodic membrane skeleton continued to mature after formation. Consistent with this notion, the autocorrelation amplitudes of the periodic βII spectrin distribution also continued to increase with time as the neuron matured (*Figure 1E*).

Assembly of axon initial segment components into the periodic membrane skeleton during late development stages

As neurons further mature, axon initial segment (AIS) starts to assemble at the axonal region proximal to the cell body. Ankyrin G is the master regulating protein for AIS assembly and recruits other
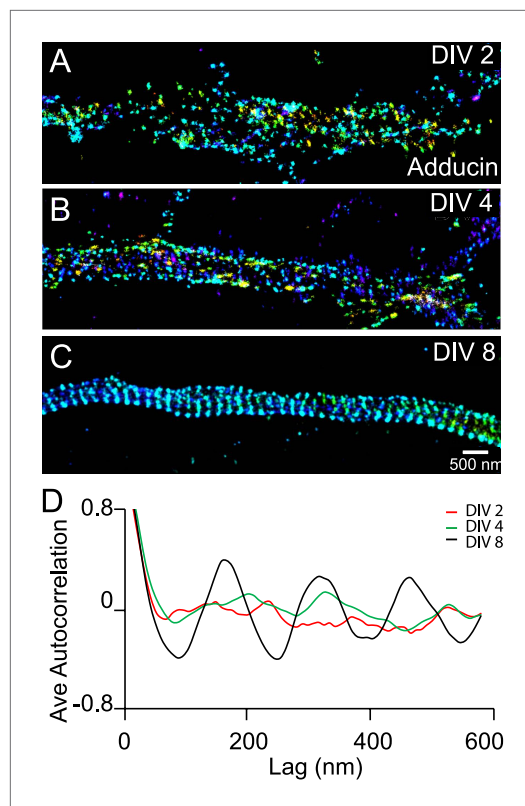
Figure 3. Recruitment of adducin into the periodic lattice structure during development. (**A**–**C**) Neurons were immunostained for adducin and imaged by 3D STORM. Shown here are representative images of adducin at proximal axonal regions from DIV 2, 4, and 8 neurons. (**D**) Average autocorrelation analyses of adducin at proximal regions of axons near the cell body. The autocorrelation curves are averaged from multiple neurons (n = 5 neurons for DIV 2; n = 7 neurons for DIV 4; n = 6 neurons for DIV 8; three independent experiments at each DIV).
DOI: 10.7554/eLife.04581.011

The following figure supplement is available for figure 3:

Figure supplement 1. Distribution of adducin in axons.
DOI: 10.7554/eLife.04581.012

molecular components such as βIV spectrin and sodium channels to the AIS (*Zhou et al., 1998*; *Jenkins and Bennett, 2001*; *Yang et al., 2007*). Next, we examined whether βIV spectrin and ankyrin G were also recruited to the periodic membrane skeleton and, if so, during which developmental stage these components were incorporated.

We labeled ankyrin G using an antibody against its spectrin-binding domain near the N-terminus and βIV spectrin using an antibody against its N-terminal domain. Both ankyrin G and βIV spectrin signals were weak during early developmental stages, and the signals became stronger in the proximal region of axons at DIV 8 (*Figure 4—figure supplement 1*). Notably, the expression level of βII spectrin remained high throughout the axons during this time (*Figure 4—figure supplement 1*). At this time, the distributions of ankyrin G and βIV spectrin were not periodic (*Figure 4A–D*), in contrast to the highly periodic βII spectrin in the proximal region of axons (*Figure 1*). Over time, both ankyrin G and βIV spectrin signals further increased in the proximal region of axons, and by DIV 12, the N-terminal domains of both ankyrin G and βIV spectrin adopted highly periodic distributions, indicating that these molecules were incorporated into the periodic lattice structure (*Figure 4A–D*). Interestingly, the periodicity was substantially less pronounced for the C-terminal domain of βIV spectrin and undetectable for the C-terminal domain of ankyrin G (*Figure 4A–D*). These results suggest that the N-terminal regions of these molecules were tightly incorporated in the periodic lattice structure, but their C-terminal regions were likely hanging off from the lattice structure and moving relatively freely. Notably, as ankyrin G and βIV spectrin became incorporated into the periodic lattice, we observed a decrease in the local concentration of βII spectrin at the AIS (*Figure 4E* and *Figure 4—figure supplement 1C*). The decrease of the βII spectrin concentration was associated with a loss of periodicity for βII spectrin at AIS (*Figure 4F*), suggesting that as βIV spectrin was incorporated into the periodic structure in the AIS region, βII spectrin was displaced.

To test whether the assembly of βIV spectrin into the periodic structure may rely on βII spectrin, we knocked down βII spectrin at various DIVs using a shRNA-expressing adenovirus, which also expressed GFP, and subsequently imaged βIV spectrin at DIV 12. The efficiency of knockdown was demonstrated by a lack of βII spectrin signal in virus-infected, GFP-positive neurons (*Figure 4—figure supplement 2*). When infected by the virus at DIV 3, the enrichment of βIV spectrin in the AIS region appeared partially impaired by βII spectrin knockdown, though at least 60% of the neurons still exhibited enrichment of βIV spectrin in AIS. For these neurons, the periodicity of βIV spectrin was also partially disrupted in the βII spectrin-depleted neurons (*Figure 4—figure supplement 2A–C*), indicating that βII spectrin is important for the periodic assembly of βIV spectrin. On the other hand, when neurons were infected with the virus at DIV 7, βIV spectrin remained periodic even though βII spectrin was depleted (*Figure 4—figure supplement 2D–F*). Because it takes several days for pre-existing βII spectrin molecules to degrade
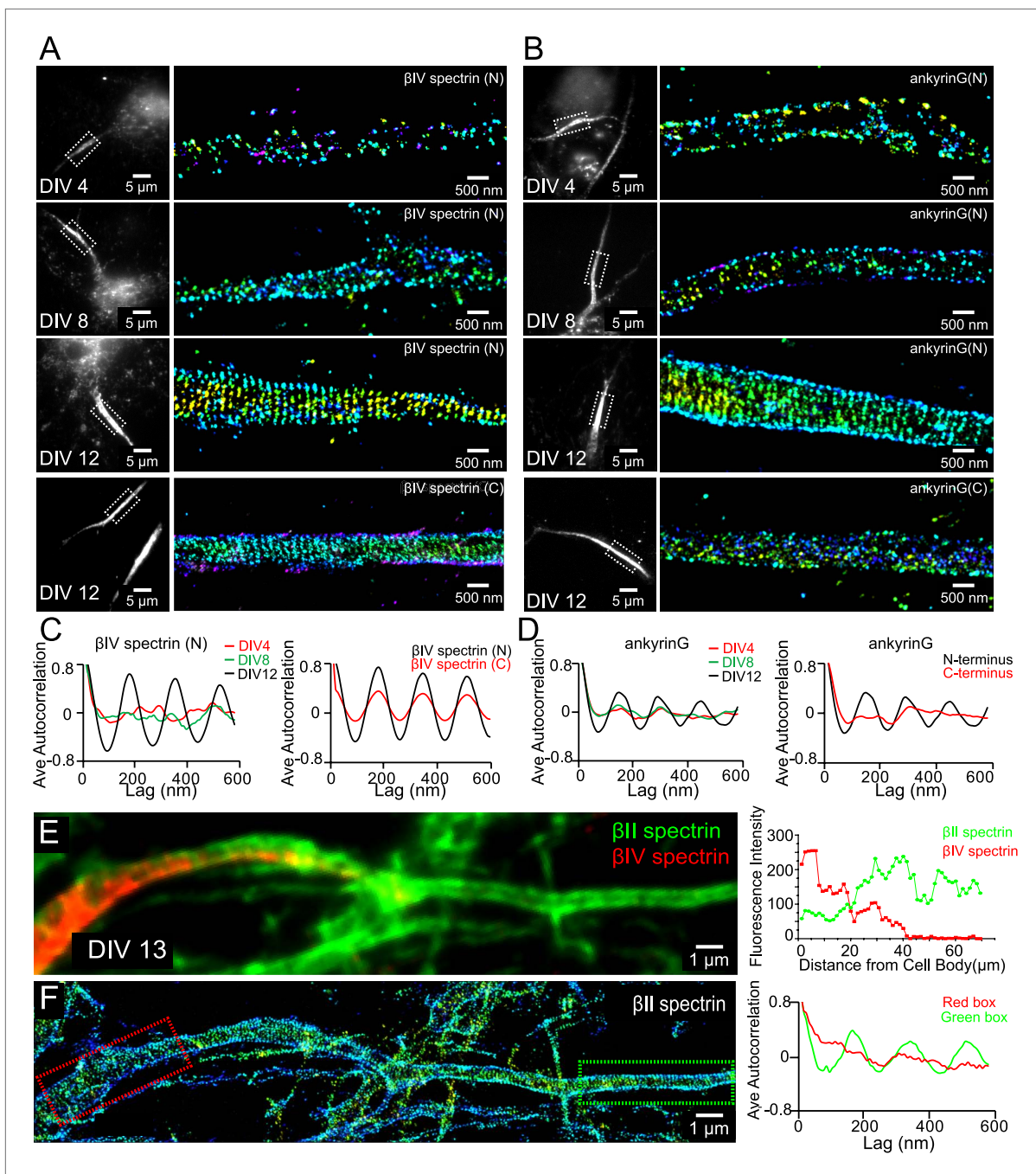
Figure 4. Assembly of AIS components into the periodic lattice structure during late developmental stages. (**A** and **B**) Neurons were immunostained with antibodies against βIV spectrin N-terminus (βIV spectrin (N)), βIV spectrin C-terminus (βIV spectrin (C)), ankyrin G spectrin-binding domain (ankyrin G (N)), or ankyrin G C-terminus (ankyrin G (C)), and imaged at various DIVs by 3D STORM. Representative conventional images and STORM images from the boxed region at different developmental stages are shown. (**C**) Left: average autocorrelation analyses of βIV spectrin N-terminus from neurons at different developmental stages (n = 9 neurons for DIV 4; n = 12 neurons for DIV 8; n = 16 neurons for DIV 12; at least three independent experiments at each DIV). Right: average autocorrelation analyses of βIV spectrin N-terminus and C-terminus of DIV 12 neurons (n = 13 neurons for N-terminus and n = 15 neurons for C-terminus, three independent experiments). (**D**) Left: average autocorrelation analyses of ankyrin G spectrin-binding domain (near N-terminus) from neurons at different developmental stages (n = 12 neurons for DIV 4; n = 15 neurons for DIV 8; n = 14 neurons for DIV 12; at least three independent experiments at each DIV). Right: average autocorrelation analysis of ankyrin G N-terminus and C-terminus of DIV 12 neurons (n = 9 neurons for N-terminus and n = 10 neurons for C-terminus, three independent experiments). (**E** and **F**) A DIV 13 neuron was immunostained with βIV and βII spectrin antibodies. βII spectrin was subjected for 3D STORM imaging. (**E**) Left: conventional image of βII and βIV spectrin in axon. Right: fluorescent

Figure 4. Continued on next page

(*Susuki et al., 2011*), it is likely that βIV spectrin was already incorporated into the periodic lattice before the eventual depletion of βII spectrin when the virus was added late.

Stability of the periodic membrane skeleton

We next probed the dynamics of the periodic lattice structure in live neurons. To this end, we genetically fused βII spectrin with mMaple3, a recently developed photoactivatable fluorescent protein (*Wang et al., 2014*). In neurons moderately expressing βII spectrin-mMaple3, the periodic pattern of βII spectrin-mMaple3 was readily observable in axons and the spacing of ~190 nm was identical to that observed for endogenous βII spectrin in fixed neurons (*Figure 5A*). The periodic pattern was smeared in neurons with high expression levels of βII spectrin-mMaple3, presumably by the excess, freely diffusing βII spectrin-mMaple3 molecules that were not incorporated into the lattice structure.

The periodic βII spectrin pattern appeared to be mostly static. Fourier analysis of the patterns showed that the spatial frequency (i.e., the period) of the structure did not change over the imaging time of several minutes (*Figure 5B*). Cross-correlation analysis of the patterns taken at different time points showed no phase shift of the periodic structure during the imaging time (*Figure 5C*).

As an alternative approach to probe the stability of the structure, we used fluorescence recovery after photo-bleaching (FRAP). For this analysis, we transfected neurons with a βII spectrin-GFP fusion construct, bleached the GFP signal in local regions of axons, and measured the signal recovery rate. In neurons that exhibited moderate expression levels of βII spectrin, where the majority of βII spectrin-GFP molecules were incorporated into the periodic lattice structure (*Figure 5—figure supplement 1*), the recovery rate was extremely slow and essentially undetectable after 30 min (*Figure 5D*). In contrast, the fluorescence recovery was much faster (75% recovery in 5 min) in neurons, where the expression level of βII spectrin-GFP was high and the majority of βII spectrin-GFP molecules were not incorporated into the periodic structure (*Figure 5E* and *Figure 5—figure supplement 1*). These data indicate that periodic lattice structure was highly stable in live neurons.

Microtubule dependence of the periodic membrane skeleton

Microtubules are essential for the establishment of neuronal polarity. Local stabilization of microtubules is sufficient to induce axon formation (*Witte et al., 2008*). Moreover, tubulin binds to ankyrin B, a molecule that also interacts with βII spectrin (*Bennett and Davis, 1981*). We thus tested whether microtubules play a role in the formation of the periodic membrane skeleton structure. In neurons treated with the microtubule-disrupting drug nocodazole (50 μM for 1 hr), the periodic pattern of βII spectrin was largely disrupted (*Figure 6A,B*). On the other hand, when microtubules were stabilized with taxol (5 nM for 3 days), a treatment that is known to induce multiple axon-like processes in neurons (*Witte et al., 2008*), we found that βII spectrin exhibited a periodic pattern in all of these axon-like processes (*Figure 6C*). We also treated neurons with SB 216763, a drug that stabilizes microtubules and promotes axonal growth by inhibiting glycogen synthase kinase-3 beta (GSK-3β) (*Jiang et al., 2005*; *Yoshimura et al., 2005*). Similarly, in neurons treated with SB-216763, we observed that the periodic lattice structure was formed in multiple axon-like long processes (*Figure 6—figure supplement 1*).

Role of ankyrin B in the periodic membrane skeleton

Given the dramatically different actin–spectrin organizations in axons and dendrites, an interesting question arises as to what molecular factors are critical for promoting the formation of the highly regular, periodic lattice structure in axons and/or suppressing it in dendrites. Ankyrin B (ANK 2) is a molecule that binds to βII spectrin (*Bennett and Lorenzo, 2013*). It is highly enriched in axons
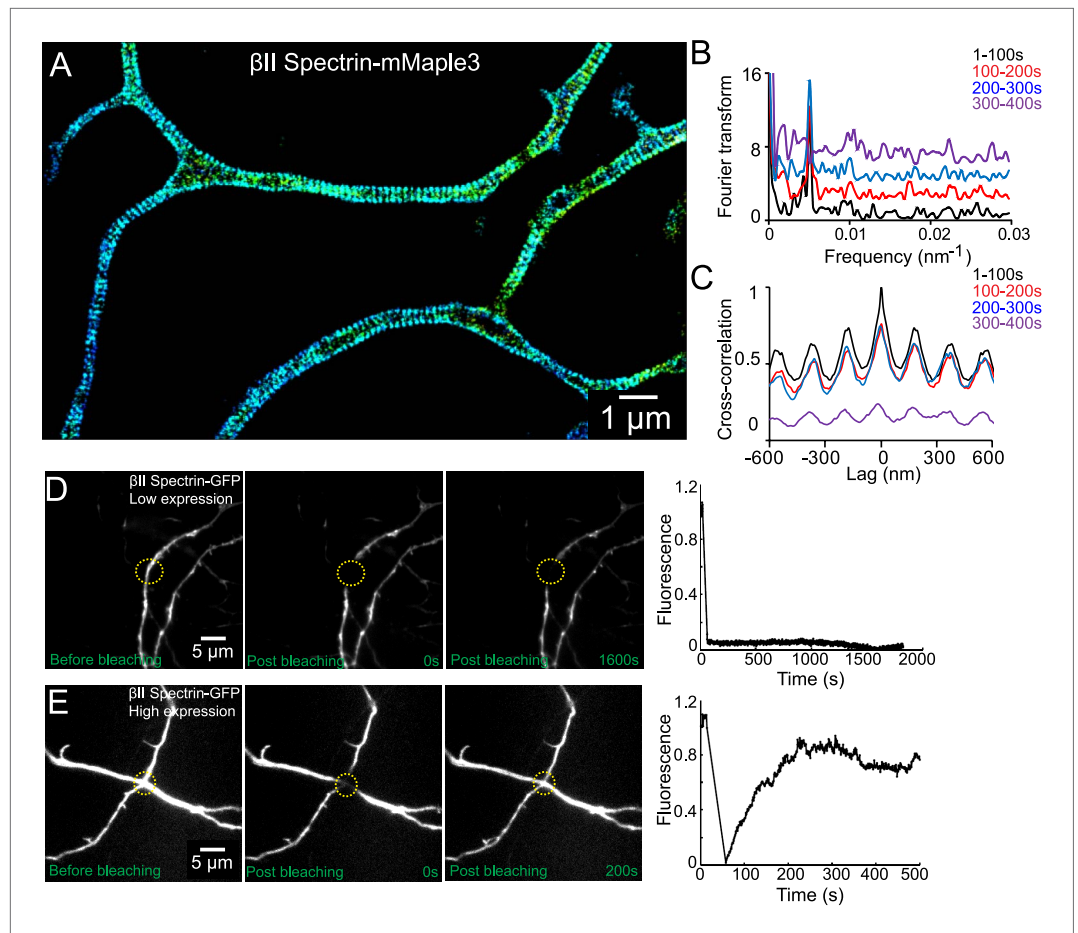
Figure 5. The periodic lattice structure is stable in live neurons. (**A**) 3D STORM image of βII spectrin-mMaple3 in live neurons at DIV 10. (**B**) The STORM movie was segregated into four different time windows. Fourier transform analysis of each time window is shown. The baseline of Fourier traces is shifted manually for clear visualization. (**C**) Cross-correlation analysis of βII spectrin across different time windows. The black curve is the autocorrelation of the image during 0–100 s. The color curves are the cross-correlation between 0–100 s and later time windows. Similar results were found in six independent experiments. (**D–E**) FRAP analyses of βII spectrin in DIV 10 neurons. Neurons were transfected with βII spectrin-GFP at DIV 8. (**D**) Representative neurons at a low βII spectrin expression level, where βII spectrin-GFP molecules were incorporated into the periodic structure. The images before photo-bleaching, 0 s post-bleaching, 1600 s post-bleaching, and the fluorescence recovery trace are shown. (**E**) The fluorescence recovery of representative neurons with a high βII spectrin expression level, where most βII spectrin-GFP molecules were not incorporated into the periodic structure. Similar results were found in at least nine independent experiments.

The following figure supplement is available for figure 5:

Figure supplement 1. Incorporation of βII spectrin-GFP into the periodic lattice structure in overexpressing neurons.

(**Chan et al., 1993**; **Kunimoto, 1995**; **Engelhardt et al., 2013**) and recently found to be potentially linked with autism (**De Rubeis et al., 2014**; **Iossifov et al., 2014**). We have shown previously that ankyrin B also adopts a partially periodic pattern in axons albeit with a lower regularity (**Xu et al., 2013**), potentially due to an incomplete occupancy of the ankyrin B binding sites on the lattice structure and the presence of ankyrin B on intracellular membranes (**Bennett and Lorenzo, 2013**). We thus asked whether ankyrin B is involved in regulating the formation of this periodic membrane skeleton in axons.

To address this question, we performed STORM imaging on disassociated hippocampal neurons from ankyrin B knockout mice (**Scotland et al., 1998**) at DIV 10. Similar to wild-type neurons, ankyrin B knockout neurons still showed enrichment of MAP2 in dendrites with similar dendritic morphology,
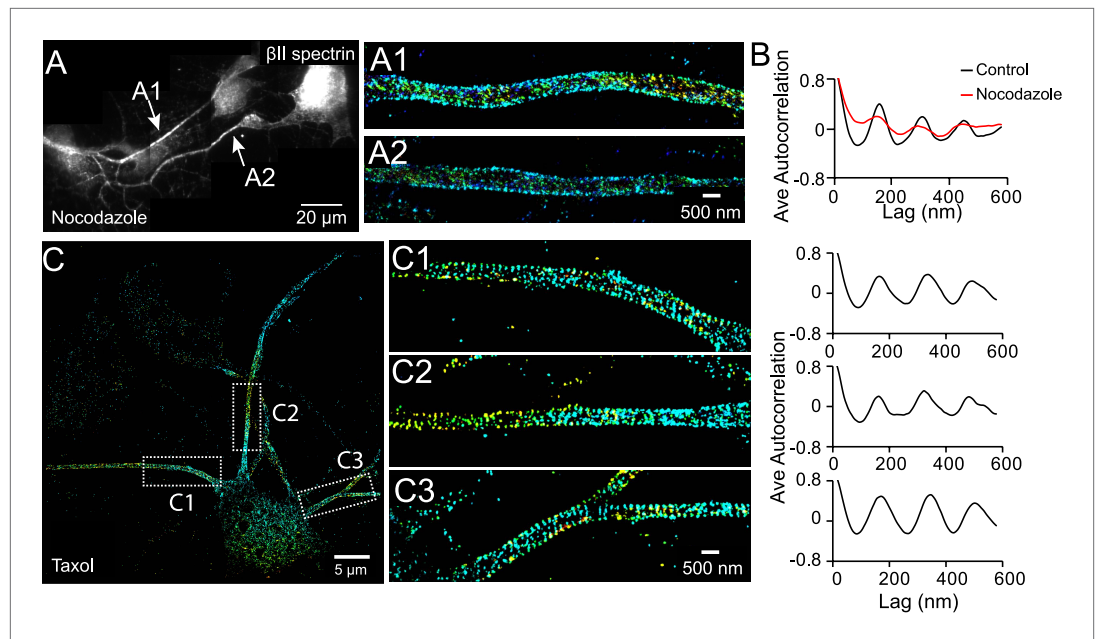
Figure 6. The periodic structure of βII spectrin relies on intact microtubules. (**A** and **B**) DIV 4 neurons were either untreated or treated with nocodazole (50 μM) for 1 hr and immunostained with βII spectrin antibody for 3D STORM. A reconstructed neuron image from nocodazole-treated neurons and two STORM images are shown in **A**. (**B**) Average autocorrelation analyses of βII spectrin from multiple control and nocodazole-treated neurons (n = 9 neurons for control and n = 8 neurons for nocodazole-treated conditions; three independent experiments for each condition). (**C**) Neurons were treated with taxol (5 nM) at DIV 3 for 3 days, which induces the growth of multiple axon-like processes. A representative STORM image of a treated neuron at DIV 6, the enlarged images of the boxed regions, and the autocorrelation analyses (n = 10 neurons, four independent experiments) are shown.
DOI: 10.7554/eLife.04581.018

The following figure supplement is available for figure 6:

Figure supplement 1. The periodic βII spectrin structure can be induced in multiple processes by axon-promoting small molecules.
DOI: 10.7554/eLife.04581.019

making dendrites easy to identify in these neurons (*Figure 7A* and *Figure 7—figure supplement 1*). The periodic pattern of βII spectrin in axons was not perturbed by ankyrin B deletion and appeared quantitatively similar to that observed in control wild-type neurons (*Figure 7—figure supplement 1*). Surprisingly, βII spectrin also adopted a highly regular, periodic distribution in all dendrites, with the periodicity quantitatively similar to that observed in axons (*Figure 7A,B*). This is in stark contrast to what we observed in wild-type neurons, where the distributions of βII spectrin in dendrites were largely irregular (*Figure 1—figure supplement 5*). The actin-capping protein adducin also adopted a periodic distribution in dendrites of ankyrin B knockout neurons, with quantitatively similar periodicity to that of βII spectrin. Knocking-down βII spectrin disrupted the periodic distribution of adducin, indicating that the periodic lattice structure in the dendrites of the ankyrin B knockout neurons also depended on βII spectrin (*Figure 7—figure supplement 2*). These data indicate that the formation of the periodic membrane skeleton does not require ankyrin B. Instead, ankyrin B is important for inhibiting the formation of this periodic lattice structure in dendrites.

Local βII spectrin concentration regulates the formation of this periodic lattice structure, and ankyrin B regulates the polarized distribution of βII spectrin in neurites

In addition to the induction of the periodic lattice structure in dendrites, we noticed that ankyrin B knockout also induced a dramatic redistribution of βII spectrin in neurites. In wild-type neurons, the local concentration of βII spectrin, as indicated by immunofluorescence intensity, was ~twofold higher in axons than that in dendrites (*Figure 7C,D*), consistent with previous results (*Riederer et al., 1986*; *Galiano et al., 2012*). However, the expression level of βII spectrin was substantially increased in
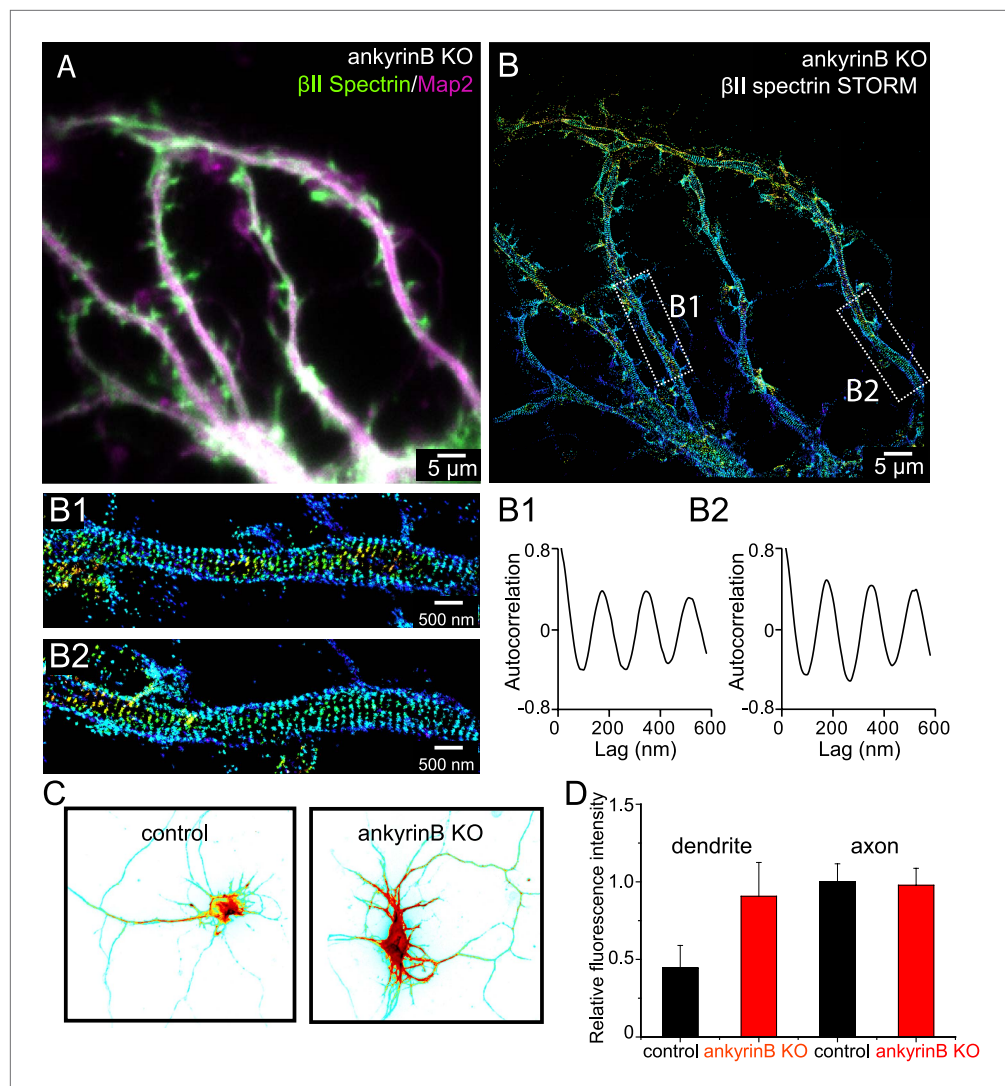
Figure 7. Role of ankyrin B in the regulation of the periodic lattice structure. (**A–B**) DIV 10 neurons from ankyrin B knockout (KO) mice were immunostained for βII spectrin and a dendritic marker Map2 and imaged. (**A**) Conventional image of βII spectrin and Map2. (**B**) 3D STORM of βII spectrin. The image is taken from the green-boxed region of the neuron in **Figure 7—figure supplement 1**. The enlarged STORM image and autocorrelation analyses of boxed regions are shown in (**B1**) and (**B2**). Similar results were found in four independent experiments. (**C**) Conventional βII spectrin image from wild-type (control) and ankyrin B KO DIV 10 neurons. The fluorescence intensity is coded by color, with red indicating higher expression. (**D**) The relative fluorescence intensity of βII spectrin in dendrites and axons of wild-type and ankyrin B KO neurons (n = 14 neurons for wild-type and n = 13 neurons for ankyrin B KO; three independent experiments).

DOI: 10.7554/eLife.04581.020

The following figure supplements are available for figure 7:

Figure supplement 1. The βII spectrin structure in axons of ankyrin B KO neurons.
DOI: 10.7554/eLife.04581.021

Figure supplement 2. Formation of the periodic lattice structure in dendrites of ankyrin B knockout neurons depends on βII spectrin.
DOI: 10.7554/eLife.04581.022

dendrites by the ankyrin B knockout to a point that the local concentration of βII spectrin in dendrites became indistinguishable from that in axons, and both were comparable to the βII spectrin concentration observed in wild-type axons (**Figure 7C,D**). We thus hypothesized that the increased local concentration of βII spectrin caused the formation of this periodic lattice structure in dendrites.

To test this hypothesis, we increased the expression level of βII spectrin in all neurites by transiently transfecting neurons with a HA-tagged βII spectrin construct and performed STORM imaging on βII spectrin in transfected neurons at DIV 11. As expected, the local concentration of βII spectrin in the dendrites of βII spectrin-HA expressing neurons was higher than that observed in control neurons that did not express βII spectrin-HA (*Figure 8A–C*). Remarkably, whereas βII spectrin appeared mostly irregular in the dendrites of control neurons (*Figure 8D,E*), in βII spectrin-HA overexpressing neurons, βII spectrin displayed a periodic pattern in nearly all dendritic processes (*Figure 8F,G*). Autocorrelation analysis showed that the periodicity in the dendrites of overexpressing neurons was substantially enhanced compared to the dendrites of control neurons (*Figure 8H*).

Taken together, these data suggest that the local concentration of βII spectrin is a key determining factor for the formation of the periodic membrane skeleton in axons and that ankyrin B was critical for setting the polarized distribution of βII spectrin in axons and dendrites.

Discussion

Actin, spectrin, and associated molecules form a periodic lattice structure with long-range order underneath the axonal membrane. Many molecular components, including actin, βII spectrin, adducin,
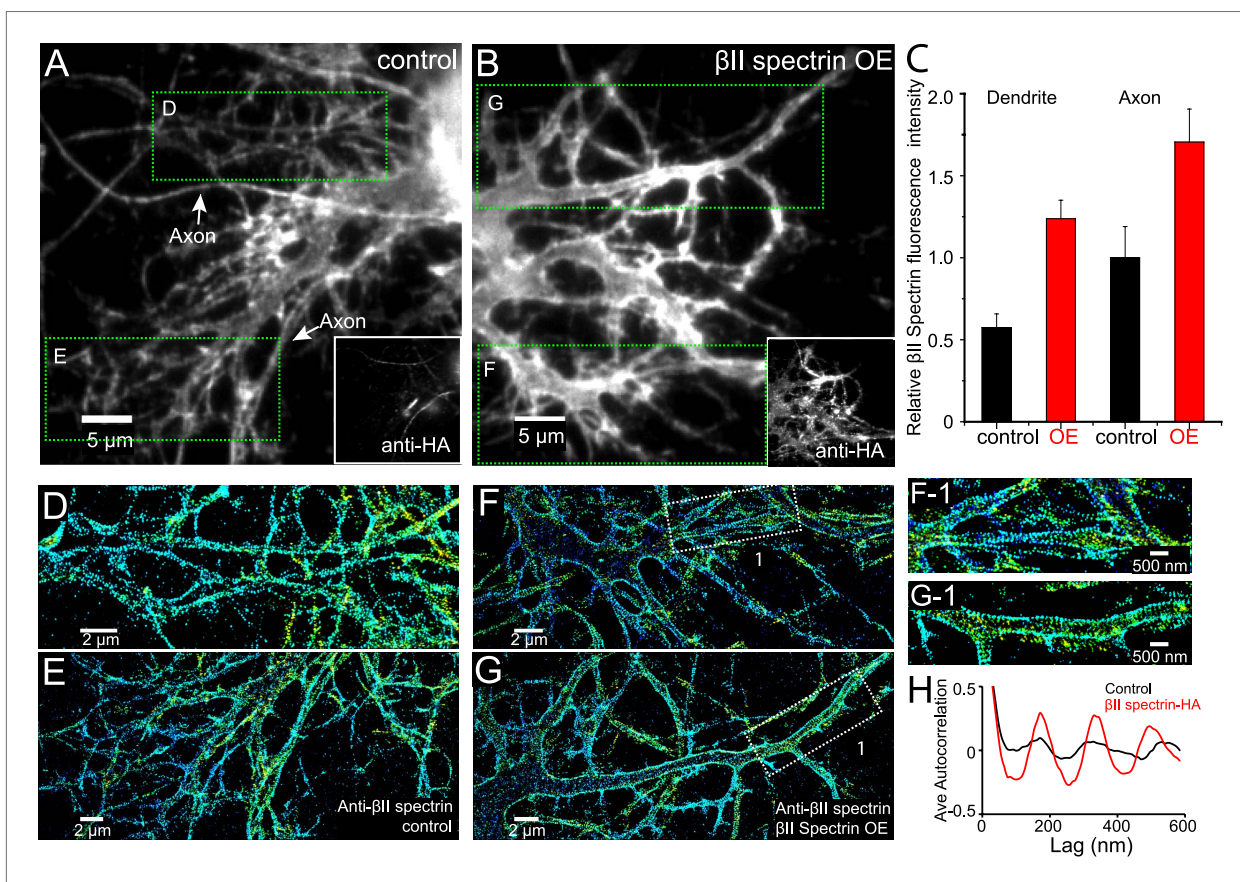

Figure 8. Local βII spectrin concentration determines the formation of the periodic lattice structure. DIV 9 neurons were either mock-transfected or transfected with βII spectrin-HA and immunostained for HA and βII spectrin. βII spectrin were subsequently imaged by 3D STORM. (**A–B**) Conventional images of βII spectrin in dendrites of a control neuron and a βII spectrin-HA overexpressing (OE) neuron. The HA image is shown in the insets. (**C**) The relative fluorescence intensity for βII spectrin in dendrites and axons of control and βII spectrin-HA overexpressing neurons (n = 10 neurons for control and n = 15 neurons for βII spectrin-HA overexpressing conditions; three independent experiments for each condition). (**D–E**) STORM images of βII spectrin from green-boxed regions in **A**. (**F–G**) STORM images of βII spectrin from green-boxed regions in **B**. (**F-1**) and (**G-1**) are enlarged images of the white-boxed regions in **F** and **G**, respectively. (**H**) Average autocorrelation analyses of βII spectrin in dendrites of control and βII spectrin-HA overexpressing neurons (n = 8 neurons for control and n = 12 neurons for βII spectrin-HA overexpressing conditions; three independent experiments for each condition).
DOI: 10.7554/eLife.04581.023

ankyrin B, βIV spectrin, ankyrin G, and sodium channels, are present in this structure. We have observed this periodic membrane skeleton with STORM imaging of fixed cultured neurons (*Figure 1* and *Figure 1—figure supplements 1–3*) and fixed brain tissue slices (*Xu et al., 2013*) using actin-binding phalloidin and immunolabeling of endogenously expressed proteins, as well as in live cultured neurons using fluorescent fusion proteins (*Figure 5*). Recently, this periodic structure has also been observed in live neurons using a cell-permeable actin-binding dye and STED imaging (*Lukinavicius et al., 2014*). Since a single actin filament can interact with multiple spectrin tetramers, and a single spectrin tetramer can bind to two actin filaments, one at each end of the symmetric tetramer (*Bennett and Lorenzo, 2013*), we reason that these crosslinking interactions are responsible for the formation of the lattice structure. Indeed, depolymerizing actin filaments disrupted the periodic distribution of βII spectrin, and knocking-down of βII spectrin disrupted the periodic distribution of actin (*Figure 1—figure supplements 2–3*). Because this lattice structure is associated with the axonal membrane, proper preservation of the membrane structure is essential for observing this structure. For example, a recent electron microscopy study of the AIS in neurons that has been subjected to detergent extraction of membrane before fixation did not show such periodic membrane skeleton (*Jones et al., 2014*). Indeed when we applied the same 'fixation after membrane extraction' protocol to neurons, the structure was destroyed and not observed in STORM images (*Figure 1—figure supplement 6*). In this study, we investigated the developmental mechanism of this newly discovered axonal membrane skeleton.

We found that this periodic membrane skeleton started to form early during axon development. In stage 3 neurons at DIV 2, when one neurite just broke the symmetry and became an axon (typically several times longer than other neurites), the periodic pattern of βII spectrin already emerged (*Figure 1*). It originated in the proximal axon regions near the cell bodies and gradually propagated to the distal ends of axons (*Figure 1*). This spatial distribution is in contrast to most previously identified signaling molecules involved in axon differentiation and development, which are enriched and function at the growing tip of axons (*Arimura and Kaibuchi, 2007*; *Barnes and Polleux, 2009*; *Stiess and Bradke, 2011*; *Cheng and Poo, 2012*). After its initial appearance, the lattice structure continued to mature with the actin filaments becoming more stable, potentially because of capping by adducin (*Figures 2, 3*). Once matured, the structure appeared highly stable with little movement and extremely slow turnover of its molecular components was observed in live neurons (*Figure 5*). This highly stable membrane skeleton may function to provide a stable mechanical support for axons. Indeed, deletion of β spectrin from *C elegans* causes axons to break when the animals move (*Hammarlund et al., 2007*).

The emergence of this periodic lattice during early axon development and its origination in the proximal axon region near the cell body suggest that the periodic membrane skeleton may function as an independent mechanism for establishing or maintaining neuronal polarization in addition to the previously identified pathways that function at the distal ends of axons. However, the periodic membrane skeleton is not required for the initiation of axon differentiation because the periodic structure only started to form in stage 3, but not stage 2, a stage at which most signaling molecules for axon initiation exhibit high activity (*Arimura and Kaibuchi, 2007*; *Cheng and Poo, 2012*). Moreover, neurons depleted of βII spectrin are also capable of forming long axons (*Galiano et al., 2012*), though these axons may not be fully functional. Indeed, removal of αII or βII spectrin is embryonically lethal in mice (*Tang et al., 2003*; *Stankewich et al., 2011*) and AIS, the structure important for action potential generation, fails to assemble properly in neurons that are depleted of βII spectrin (*Galiano et al., 2012*).

Interestingly, molecules important for the specification of AIS, ankyrin G, βIV spectrin, and sodium channels were all incorporated into this periodic membrane skeleton. During the early stages of axon development, the expression levels of ankyrin G and βIV spectrin were low in the proximal axon region, which was instead occupied by the periodic lattice comprising βII spectrin (*Figure 1*). Ankyrin G and βIV spectrin began to enrich in the proximal axon region later during axon development, at ~DIV 8 (*Figure 4—figure supplement 1*), consistent with previous observations (*Galiano et al., 2012*). The incorporation of ankyrin G and βIV spectrin into the periodic lattice was observed even later, at around DIV 12, replacing βII spectrin from the structure in the AIS (*Figure 4*). The enrichment and periodic assembly of the AIS components appeared to depend on βII spectrin (*Figure 4—figure supplement 2*). Our data suggest the following developmental course for the AIS formation. Before the AIS is formed, actin and βII spectrin form a cohesive periodic lattice structure that covers the entire axonal shaft including the proximal axonal region. The AIS then forms by the enrichment of ankyrin G and βIV spectrin in the proximal axonal region and the replacement of βII spectrin by βIV spectrin in the periodic membrane skeleton. Potentially, ankyrin G, the master regulator of AIS that recruits other AIS

components (*Zhou et al., 1998*; *Jenkins and Bennett, 2001*; *Yang et al., 2007*), is first enriched in the proximal axon region. Ankyrin G then recruits βIV spectrin to the same region and causes it to be incorporated in the periodic lattice. βIV spectrin in turn anchors ankyrin G into a periodic pattern as well. As an adaptor, ankyrin G then places sodium channels into a periodic distribution pattern in the AIS.

Finally, we addressed the question why the cohesive, periodic lattice structure preferentially formed in axons, with dendrites showed at most isolated patches of periodic structure with much less regularity (*Figure 1—figure supplement 5*). We found multiple molecular factors participate in this regulation. The periodic lattice structure depended on intact microtubules. Treatment with a microtubule-depolymerizing drug disrupts the structure in axons, whereas treatment with microtubule-stabilizing drugs induces the formation of the lattice structure in multiple neurites (*Figure 6*). Importantly, we found that the local concentration of βII spectrin is a determining factor for the formation of the lattice structure. The local concentration of βII spectrin is ~2 times higher in axons than in dendrites (*Figure 7*). Remarkably, increasing the dendritic concentration of βII spectrin by overexpression induced the formation of the periodic lattice structure in all dendrites (*Figure 8*). Interestingly, ankyrin B was critical for maintaining the polarized distribution of βII spectrin. Knocking out ankyrin B led to an even distribution of βII spectrin in dendrites and axons and the formation of a highly regular and cohesive periodic lattice structure in all dendrites (*Figure 7*). Consistent with the notion that the increased concentration of βII spectrin in dendrites is responsible for inducing the formation of the periodic lattice structure in dendrites, knocking-down βII spectrin from ankyrin B knockout neurons disrupted the lattice structure (*Figure 7—figure supplement 2*). These results indicate that ankyrin B is critical for establishing a polarized distribution of βII spectrin in neurites with a higher concentration of βII spectrin in axons than in dendrites, which in turn promotes the formation of the periodic membrane skeleton in axons.

It is interesting to speculate how ankyrin B may establish such a polarized distribution of βII spectrin. The predominant form of ankyrin B during early neuronal development is a 440-kDa splice variant that is preferentially targeted to axons (*Kunimoto et al., 1991*; *Chan et al., 1993*; *Kunimoto, 1995*). Given that ankyrin B specifically binds to βII spectrin, we speculate that the distribution of ankyrin B in axons may help establishing the enrichment of βII spectrin in axons during early neuronal development. Moreover, we recently found that ankyrin B is a major cargo adaptor for dynactin and promotes axonal transport of proteins and organelles and that disruption of ankyrin B–dynactin interaction significantly impairs the axonal transport of many proteins (*Lorenzo et al., 2014*). It is thus possible that ankyrin B may also preferentially transport βII spectrin into axons instead of dendrites. By maintaining a polarized distribution of βII spectrin in neurons, ankyrin B functions as a negative regulator for preventing the formation of the periodic membrane skeleton in dendrites. The exact mechanism by which ankyrin B maintains a polarized distribution of βII spectrin remains an interesting question for future investigation.

Materials and methods

All experimental procedures were performed in accordance with the Guide for the Care and Use of Laboratory Animals of the National Institutes of Health. The protocol was approved by the Institutional Animal Care and Use Committee (IACUC) of Harvard University.

Neuron culture

Primary hippocampal cultures were prepared from wild-type neonatal (E18) rat embryos (timed pregnant SD rats from Charles River Laboratories, Wilmington, MA) or ankyrin B knockout mice as reported previously (*Scotland et al., 1998*). Hippocampi were isolated and digested with 0.05% trypsin–EDTA (1×) (Invitrogen 25300-054, Grand Island, NY) at 37°C for 15 min. The hippocampi were transferred to the Hib A solution (BrainBits HA-Ca, Springfield, IL), washed several times with the Hib A solution, and pipetted up and down until the tissues were mostly dissolved. The solution was then passed through a cell strainer (VWR 21008-949, Philadelphia, PA) to remove the residual undissociated tissue and collected in a 50 ml conical tube. Neurons were spun down to the bottom of the tube, resuspended with the culture media made of 96 ml Neurobasal (Life Technologies 12349-015), 2 ml B-27 Supplement (Life Technologies 17504-044, Grand Island, NY), 1 ml Penicillin-Streptomycin (Life technologies 15140-122) and 1 ml Glutamax (Life technologies 35050-061), and then plated onto poly-L-lysine/laminin-coated 12-mm coverslips (BD bioscience BD354087, San Jose, CA) or poly-L-lysine coated 8-well chambers. 5 µM cytosine-D-arabinofuranoside (Sigma C1768, St. Louis, MO) was added to the culture media to inhibit the growth of glial cells 3 days after plating. The neurons were fed twice a week with freshly made culture media until use.

Reagents

The following primary antibodies were used in this study: guinea pig anti-Map2 antibody (Synaptic Systems, 188002, Goettingen, Germany); mouse anti-βII spectrin antibody (BD Biosciences, 612563); mouse anti-ankyrin G antibody (Santa Cruz, Sc-12719, Dallas, Texas; epitope mapping the spectrin-binding domain of ankyrin G near the N-terminal); goat anti-ankyrin G antibody (Santa Cruz, Sc-31778, epitope mapping the C-terminal of ankyrin G); rabbit anti-adducin antibody (Abcam, ab51130, Cambridge, MA); rabbit anti-HA antibody (Abcam, ab9110); rabbit anti-GFP antibody (Abcam, ab290); goat anti-βIII spectrin (Santa Cruz, sc-9660). Rabbit antibodies targeting the C- or N-terminus of βIV spectrin were kind gifts from Dr Matt Rasband at Baylor College of Medicine.

The following secondary antibodies were used in this study for conventional imaging: Alexa Fluor 647 donkey anti-mouse (Invitrogen, A31571), Alexa Fluor 555 donkey anti-mouse (Invitrogen, A31570), Alexa Fluor 488 donkey anti-mouse (Invitrogen, A21202), Alexa Fluor 647 donkey anti-rabbit (Invitrogen, A31573), Alexa Fluor 568 donkey anti-rabbit (Invitrogen, A10042), Alexa Fluor 488 donkey anti-rabbit (Invitrogen, A21206), Alexa Fluor 488 goat anti-guinea pig (Invitrogen, A11073), Alexa Fluor 647 donkey anti-goat (Invitrogen, A21447), Alexa Fluor 568 donkey anti-goat (Invitrogen, A11057).

For STORM imaging, secondary antibodies were custom-labeled with a photoswitchable reporter dye, Alexa Fluor 647, and an activator dye Alexa Flour 405, which facilitates the photoswitching of the reporter dye. Donkey anti-mouse and donkey anti-rabbit secondary antibodies (Jackson ImmunoResearch, West Grove, PA) were each labeled with a mixture of amine-reactive activator and reporter dyes in a one-step reaction, as described previously (*He et al., 2013*). In some experiments, commercial Alexa Fluor 647 conjugated donkey anti-mouse, anti-rabbit or anti-goat secondary antibodies were used.

Transfection of neurons with fusion protein constructs

βII spectrin-GFP and βII spectrin-HA plasmids (addgene, 31070, Cambridge, MA) used in this study were reported previously, with GFP inserted at the N-terminal of βII spectrin and the HA tag at the C-terminal of βII spectrin, respectively (*Galiano et al., 2012*). To make the βII spectrin-mMaple 3 construct, we replaced the HA tag sequence with the mMaple 3 sequence (*Wang et al., 2014*). Plasmids were transfected into neurons using a calcium phosphate transfection kit from Invitrogen (K2780-01). The protocol for transfection was modified slightly for our neuronal cultures. Briefly, neurons were plated at a density of 40,000 cells/well in 12-well plates and cultured for 6–10 days before the transfection. After changing media from original neuronal culture media to Minimum Essential Media (MEM, Life Technology, supplemented with 20 mM HEPEs, pH 7.15), 100 µl plasmid mixture was added, and neurons were incubated at 37°C for 20 min. The media was subsequently aspirated and replaced with a lower pH MEM (supplemented with 20 mM HEPEs, pH 6.8) at 37°C for 4 min. After dissolving all calcium phosphate crystals, we added back the original neuronal culture media. Experiments were performed 2 or 3 days after transfection.

Knockdown with shRNA

The βII spectrin-shRNA adenoviral construct used in this study was a kind gift from Dr Matt Rasband at Baylor College of Medicine and described previously (*Hedstrom et al., 2008*). The two sense sequences of shRNA are: 5′-GCATGTCACGATGTTACAA-3′ and 5′-GGATGAAATGAAGGTGCTA-3′. For assaying the effect of βII spectrin knockdown on actin and adducin structure, neurons were infected with the virus at DIV 3 and fixed for STORM imaging at around DIV 9 or 10. For assaying the effect of βII spectrin knockdown on βIV spectrin structure, neurons were infected with the virus at DIV 3 or DIV 7 and fixed at DIV 12 for STORM imaging of βIV spectrin. Infected neurons were marked by a GFP signal expressed from the adenoviral construct. The knockdown efficiency was validated through immunostaining against βII spectrin.

Drug treatment of neurons

The following chemicals were used in this study with their concentration and treatment time stated: latrunculin A (Sigma, L5163, 20 µM, 1 hr or indicated time series), cytochalasin D (Sigma, C8273, 50 µM, 1 hr), nocodazole (Sigma, M1404, 50 µM, 1 hr), taxol (Sigma, T7402, 5 nM), SB-216763 (Sigma, S3442, 5 µM). For taxol treatment, neurons were treated with the drug at DIV 3 with the indicated concentration and fixed at DIV 6 for STORM imaging. For SB216763 treatment, neurons were treated with the drug at DIV 1 with the indicated concentration and fixed at DIV 5 for STORM imaging.

Fluorescence labeling of neurons

Cultured neurons were fixed at various days in vitro (DIV). For imaging of actin, we used a similar method to label actin as reported previously (*Koestler et al., 2008*; *Xu et al., 2013*). Briefly, the samples were simultaneously fixed and extracted for 1 min using a solution of 0.3% (vol/vol) glutaraldehyde (GA) and 0.25% (vol/vol) Triton X-100 in cytoskeleton buffer (CB, 10 mM MES, pH 6.1, 150 mM NaCl, 5 mM EGTA, 5 mM glucose, and 5 mM MgCl$_2$) and then post-fixed for 15 min in 2% (vol/vol) GA in CB, a previously established protocol for maintaining actin ultrastructure (*Koestler et al., 2008*; *Xu et al., 2013*). The GA-fixed samples were treated with freshly prepared 0.1% (wt/vol) sodium borohydride for 7 min to reduce background fluorescence caused by GA fixation. To label actin filaments, samples were labeled with Alexa Fluor 647 conjugated phalloidin (Invitrogen A22287) overnight at 4°C or ~1 hr at room temperature. A concentration of ~0.5 µM phalloidin in PBS was used. To minimize the dissociation of phalloidin from actin during washing steps, actin labeling was performed after all other labeling steps (i.e., immunofluorescence of other molecular targets) were completed. The sample was washed 2–3 times with PBS and then immediately mounted for imaging.

To test whether strong membrane extraction prior to fixation (*Jones et al., 2014*) disrupts the membrane skeleton structure, neurons were extracted with 1% Triton X-100 in PEM buffer (100 mM Pipes–KOH, pH 6.9, 1 mM MgCl$_2$, and 1 mM EGTA) containing 2% polyethylene glycol, 2 µM phalloidin, and 2 µM taxol for 3 min at room temperature after a quick rinse with the PEM buffer containing 2 µM taxol and subsequently fixed with 0.2% GA in PBS for at least 20 min, as described previously (*Jones et al., 2014*). Fixed samples were treated with freshly prepared 0.2% (wt/vol) sodium borohydride for 5–10 min to reduce background fluorescence caused by GA fixation and washed in PBS. Actin labeling was performed similarly as described above.

For imaging of molecular components not including actin (MAP2, βII spectrin, βIII spectrin, βIV spectrin, ankyrin G, and adducin), the samples were fixed using 4% (wt/vol) paraformaldehyde in phosphate buffered saline (PBS) for 15 min. Fixed neuron samples were then permeabilized and blocked in blocking buffer (3% wt/vol bovine serum albumin or 10% wt/vol donkey serum, 0.2% vol/vol Triton X-100 in PBS) for 1 hr and subsequently stained with primary antibodies in blocking buffer overnight at 4°C. The samples were washed three times and then stained with secondary antibodies (described above) in blocking buffer for ~1 hr at room temperature.

Fixed-cell STORM imaging

The imaging buffer was PBS containing 100 mM cysteamine, 5% glucose, 0.8 mg/ml glucose oxidase (Sigma-Aldrich), and 40 µg/ml catalase (Roche Applied Science, Indianapolis, IN) for fixed neurons. To image the samples from 12-mm coverslips, approximately 4 µl of imaging buffer was dropped at the center of a freshly-cleaned #1.5 rectangular coverslip (22 mm by 60 mm), and the sample on the 12-mm coverslip was mounted on the rectangular coverslip and sealed with nail polish or Cytoseal. To image samples from 8-well chambers, 400 µl of imaging buffer was added to the imaging chamber.

The STORM setup was based on an Olympus IX-71 inverted optical microscope as described previously (*Jones et al., 2011*). 405-nm (CUBE 405-50C; Coherent, Santa Clara, CA), 460-nm (Sapphire 460-10; Coherent), 532-nm (GCL-200-I; CrystaLaser, Reno, NV), and 657-nm (RCL-300-656; CrystaLaser) lasers were introduced into the sample through the back focal plane of the microscope. A translation stage allowed the laser beams to be shifted towards the edge of the objective so that the emerging light reached the sample at incidence angles slightly smaller than the critical angle of the glass–water interface, thus illuminating only the fluorophores within a few micrometers of the coverslip surface. A T660LPXR (Chroma, Bellows Falls, VT) was used as the dichroic mirror and an ET705/72M bandpass filter (Chroma) was used as the emission filter. For 3-dimensional (3D) STORM imaging, a cylindrical lens was inserted into the imaging path so that images of single molecules were elongated in *x* and *y* for molecules on the proximal and distal sides of the focal plane (relative to the objective), respectively (*Huang et al., 2008*).

During imaging, continuous illumination of 657-nm laser (~2 kW/cm^2) was used to excite fluorescence from Alexa Flour 647 molecules and switched them into the dark state. Continuous illumination of the 405-nm laser (when Alexa Flour 405 was used as the activator dye) or 532-nm laser (when Cy3 was used as the activator dye) was used to reactivate the fluorophores to the emitting state. The power of the activation lasers (typical range 0–1 W/cm^2) was adjusted during image acquisition so that at any given instant, only a small, optically resolvable fraction of the fluorophores in the sample was in the emitting state.

A typical STORM image was generated from a sequence of about 30,000–60,000 image frames at a frame rate of 60 Hz. The recorded STORM movie was analyzed according to previously described methods (*Rust et al., 2006*; *Huang et al., 2008*). The centroid positions and ellipticities of the single molecule images provided lateral and axial positions of each activated fluorescent molecule, respectively (*Huang et al., 2008*). Super-resolution images were reconstructed from the molecular coordinates by depicting each location as a 2D Gaussian peak.

Live-cell STORM imaging

Live-cell STORM experiments were performed on the same STORM setup as described earlier (*Jones et al., 2011*; *Shim et al., 2012*). Neurons were initially transfected with βII spectrin-mMaple 3 at DIV 8 and imaged in an extracellular solution containing: 128 mM NaCl, 5 mM KCl, 2 mM $CaCl_2$, 1 mM $MgCl_2$, 25 mM HEPES, 30 mM glucose, pH 7.3 at DIV 10 or DIV 11. Continuous illumination of the 405-nm laser was used to activate the mMaple 3 fluorescent protein. Continuous illumination of 561-nm laser was used to excite mMaple 3 and switched them to the dark state. Imaging analysis was performed as described above.

FRAP analysis

FRAP experiments were performed on the same STORM setup as described above. Neurons were transfected with βII spectrin-GFP at DIV 8 and then imaged at DIV 10. Directly before FRAP experiments, neuronal culture media were replaced with an extracellular solution. After recording an image before photo-bleaching, a small region of the sample was bleached by shrinking the size of iris at the excitation light path for 10 s with the maximum laser power. Subsequently, the sample was imaged using the same power as that of pre-bleached image. The image was recorded at a frequency of 1 Hz. We used the unbleached regions in the image to calibrate the photo-bleaching effect during the entire recording time. The fluorescence recovery fraction was measured as the fluorescence intensity at the bleached region at indicated time vs the original intensity before photo-bleaching.

Acknowledgements

Additional information

Competing interests

XZ: Reviewing editor, *eLife*. The other authors declare that no competing interests exist.

Funding

Author contributions

GZ, JH, Conception and design, Acquisition of data, Analysis and interpretation of data, Drafting or revising the article, Contributed unpublished essential data or reagents; RZ, Acquisition of data, Analysis and interpretation of data, Drafting or revising the article; DL, Provided the dissociated neurons from the ankyrin B knockout and control mice; HPB, Acquisition of data, Drafting or revising the article; VB, Analysis and interpretation of data, Drafting or revising the article; XZ, Conception and design, Analysis and interpretation of data, Drafting or revising the article

Ethics

Animal experimentation: This study was performed in strict accordance with the recommendations in the Guide for the Care and Use of Laboratory Animals of the National Institutes of Health. All of the animals were handled according to approved institutional animal care and use committee (IACUC) protocol, number 10-16. The protocol was approved by the Committee on the Use of Animals in Research and Teaching of Harvard University Faculty of Arts & Sciences (HU/FAS). The HU/FAS animal care and use program is AAALAC International accredited, has a PHS Assurance (A3593-01) on file with NIH's Office of Laboratory Animal Welfare, and is registered with the USDA (14-R-0128). Animals were euthanized in accordance with AVMA Guidelines for the Euthanasia of Animals.

References

Arimura N, Kaibuchi K. 2007. Neuronal polarity: from extracellular signals to intracellular mechanisms. *Nature Reviews Neuroscience* **8**:194–205. doi: 10.1038/nrn2056.

Barnes AP, Polleux F. 2009. Establishment of axon-dendrite polarity in developing neurons. *Annual Review of Neuroscience* **32**:347–381. doi: 10.1146/annurev.neuro.31.060407.125536.

Bennett V, Davis J. 1981. Erythrocyte ankyrin: immunoreactive analogues are associated with mitotic structures in cultured cells and with microtubules in brain. *Proceedings of the National Academy of Sciences of USA* **78**:7550–7554. doi: 10.1073/pnas.78.12.7550.

Bennett V, Lorenzo DN. 2013. Spectrin- and ankyrin-based membrane domains and the evolution of vertebrates. *Current Topics in Membranes* **72**:1–37. doi: 10.1016/B978-0-12-417027-8.00001-5.

Betzig E, Patterson GH, Sougrat R, Lindwasser OW, Olenych S, Bonifacino JS, Davidson MW, Lippincott-Schwartz J, Hess HF. 2006. Imaging intracellular fluorescent proteins at nanometer resolution. *Science* **313**:1642–1645. doi: 10.1126/science.1127344.

Bradke F, Dotti CG. 1999. The role of local actin instability in axon formation. *Science* **283**:1931–1934. doi: 10.1126/science.283.5409.1931.

Byers TJ, Branton D. 1985. Visualization of the protein associations in the erythrocyte membrane skeleton. *Proceedings of the National Academy of Sciences of USA* **82**:6153–6157. doi: 10.1073/pnas.82.18.6153.

Chan W, Kordeli E, Bennett V. 1993. 440-Kd Ankyrin(B) - structure of the major developmentally-regulated domain and selective localization in Unmyelinated axons. *Journal of Cell Biology* **123**:1463–1473. doi: 10.1083/jcb.123.6.1463.

Cheng PL, Poo MM. 2012. Early events in axon/dendrite polarization. *Annual Review of Neuroscience* **35**:181–201. doi: 10.1146/annurev-neuro-061010-113618.

Cingolani LA, Goda Y. 2008. Actin in action: the interplay between the actin cytoskeleton and synaptic efficacy. *Nature Reviews Neuroscience* **9**:344–356. doi: 10.1038/nrn2373.

De Rubeis S, He X, Goldberg AP, Poultney CS, Samocha K, Cicek AE, Kou Y, Liu L, Fromer M, Walker S, Singh T, Klei L, Kosmicki J, Shih-Chen F, Aleksic B, Biscaldi M, Bolton PF, Brownfeld JM, Cai J, Campbell NG, Carracedo A, Chahrour MH, Chiocchetti AG, Coon H, Crawford EL, Curran SR, Dawson G, Duketis E, Fernandez BA, Gallagher L, Geller E, Guter SJ, Hill RS, Ionita-Laza J, Jimenz Gonzalez P, Kilpinen H, Klauck SM, Kolevzon A, Lee I, Lei I, Lei J, Lehtimäki T, Lin CF, Ma'ayan A, Marshall CR, McInnes AL, Neale B, Owen MJ, Ozaki N, Parellada M, Parr JR, Purcell S, Puura K, Rajagopalan D, Rehnström K, Reichenberg A, Sabo A, Sachse M, Sanders SJ, Schafer C, Schulte-Rüther M, Skuse D, Stevens C, Szatmari P, Tammimies K, Valladares O, Voran A, Li-San W, Weiss LA, Willsey AJ, Yu TW, Yuen RK, DDD Study, Homozygosity Mapping Collaborative for Autism, UK10K Consortium, Cook EH, Freitag CM, Gill M, Hultman CM, Lehner T, Palotie A, Schellenberg GD, Sklar P, State MW, Sutcliffe JS, Walsh CA, Scherer SW, Zwick ME, Barett JC, Cutler DJ, Roeder K, Devlin B, Daly MJ, Buxbaum JD. 2014. Synaptic, transcriptional and chromatin genes disrupted in autism. *Nature* **515**:209–215. doi: 10.1038/nature13772.

Dent EW, Gertler FB. 2003. Cytoskeletal dynamics and transport in growth cone motility and axon guidance. *Neuron* **40**:209–227. doi: 10.1016/S0896-6273(03)00633-0.

Dotti CG, Sullivan CA, Banker GA. 1988. The establishment of polarity by hippocampal neurons in culture. *The Journal of Neuroscience* **8**:1454–1468.

Engelhardt M, Vorwald S, Sobotzik JM, Bennett V, Schultz C. 2013. Ankyrin-B structurally defines terminal microdomains of peripheral somatosensory axons. *Brain Structure & Function* **218**:1005–1016. doi: 10.1007/s00429-012-0443-0.

Galiano MR, Jha S, Ho TS, Zhang C, Ogawa Y, Chang KJ, Stankewich MC, Mohler PJ, Rasband MN. 2012. A distal axonal cytoskeleton forms an intra-axonal boundary that controls axon initial segment assembly. *Cell* **149**:1125–1139. doi: 10.1016/j.cell.2012.03.039.

Gao Y, Perkins EM, Clarkson YL, Tobia S, Lyndon AR, Jackson M, Rothstein JD. 2011. beta-III spectrin is critical for development of purkinje cell dendritic tree and spine morphogenesis. *The Journal of Neuroscience* **31**:16581–16590. doi: 10.1523/JNEUROSCI.3332-11.2011.

Hammarlund M, Jorgensen EM, Bastiani MJ. 2007. Axons break in animals lacking beta-spectrin. *The Journal of Cell Biology* **176**:269–275. doi: 10.1083/jcb.200611117.

He J, Sun E, Bujny MV, Kim D, Davidson MW, Zhuang X. 2013. Dual function of CD81 in influenza virus uncoating and budding. *PLOS pathogens* **9**:e1003701. doi: 10.1371/journal.ppat.1003701.

Hedstrom KL, Ogawa Y, Rasband MN. 2008. AnkyrinG is required for maintenance of the axon initial segment and neuronal polarity. *The Journal of Cell Biology* **183**:635–640. doi: 10.1083/jcb.200806112.

Hess ST, Girirajan TP, Mason MD. 2006. Ultra-high resolution imaging by fluorescence photoactivation localization microscopy. *Biophysical Journal* **91**:4258–4272. doi: 10.1529/biophysj.106.091116.

Huang B, Wang W, Bates M, Zhuang X. 2008. Three-dimensional super-resolution imaging by stochastic optical reconstruction microscopy. *Science* **319**:810–813. doi: 10.1126/science.1153529.

Hulsmeier J, Pielage J, Rickert C, Technau GM, Klambt C, Stork T. 2007. Distinct functions of alpha-Spectrin and beta-Spectrin during axonal pathfinding. *Development* **134**:713–722. doi: 10.1242/dev.02758.

Ikeda Y, Dick KA, Weatherspoon MR, Gincel D, Armbrust KR, Dalton JC, Stevanin G, Dürr A, Zühlke C, Bürk K, Clark HB, Brice A, Rothstein JD, Schut LJ, Day JW, Ranum LP. 2006. Spectrin mutations cause spinocerebellar ataxia type 5. *Nature Genetics* **38**:184–190. doi: 10.1038/ng1728.

Iossifov I, O'Roak BJ, Sanders SJ, Ronemus M, Krumm N, Levy D, Stessman HA, Witherspoon KT, Vives L, Patterson KE, Smith JD, Paeper B, Nickerson DA, Dea J, Dong S, Gonzalez LE, Mandell JD, Mane SM, Murtha MT, Sullivan CA, Walker MF, Waqar Z, Wei L, Willsey AJ, Yamrom B, Lee YH, Grabowska E, Dalkic E, Wang Z, Marks S, Andrews P, Leotta A, Kendall J, Hakker I, Rosenbaum J, Ma B, Rodgers L, Troge J, Narzisi G, Yoon S, Schatz MC, Ye K, McCombie WR, Shendure J, Eichler EE, State MW, Wigler M. 2014. The contribution of de novo coding mutations to autism spectrum disorder. *Nature* **515**:216–221. doi: 10.1038/nature13908.

Jenkins SM, Bennett V. 2001. Ankyrin-G coordinates assembly of the spectrin-based membrane skeleton, voltage-gated sodium channels, and L1 CAMs at Purkinje neuron initial segments. *The Journal of Cell Biology* **155**:739–746. doi: 10.1083/jcb.200109026.

Jiang H, Guo W, Liang XH, Rao Y. 2005. Both the establishment and the maintenance of neuronal polarity require active mechanisms: critical roles of GSK-3 beta and its upstream regulators. *Cell* **120**:123–135. doi: 10.1016/j.cell.2004.12.033.

Jones SA, Shim SH, He J, Zhuang X. 2011. Fast, three-dimensional super-resolution imaging of live cells. *Nature Methods* **8**:499–508. doi: 10.1038/nmeth.1605.

Jones SL, Korobova F, Svitkina T. 2014. Axon initial segment cytoskeleton comprises a multiprotein submembranous coat containing sparse actin filaments. *The Journal of Cell Biology* **205**:67–81. doi: 10.1083/jcb.201401045.

Kapitein LC, Hoogenraad CC. 2011. Which way to go? Cytoskeletal organization and polarized transport in neurons. *Molecular and Cellular Neuroscience* **46**:9–20. doi: 10.1016/j.mcn.2010.08.015.

Koestler SA, Auinger S, Vinzenz M, Rottner K, Small JV. 2008. Differentially oriented populations of actin filaments generated in lamellipodia collaborate in pushing and pausing at the cell front. *Nature Cell Biology* **10**:306–313. doi: 10.1038/ncb1692.

Krieg M, Dunn AR, Goodman MB. 2014. Mechanical control of the sense of touch by beta-spectrin. *Nature Cell Biology* **16**:224–233. doi: 10.1038/ncb2915.

Kuhlman PA, Hughes CA, Bennett V, Fowler VM. 1996. A new function for adducin. Calcium/calmodulin-regulated capping of the barbed ends of actin filaments. *The Journal of Biological Chemistry* **271**:7986–7991. doi: 10.1074/jbc.271.14.7986.

Kunimoto M. 1995. Neuron-specific isoform of brain ankyrin, 440-kD ankyrin(B), is targeted to the axons of rat cerebellar neurons. *Journal of Cell Biology* **131**:1821–1829. doi: 10.1083/jcb.131.6.1821.

Kunimoto M, Otto E, Bennett V. 1991. A new 440-Kd isoform is the major ankyrin in neonatal rat-brain. *Journal of Cell Biology* **115**:1319–1331. doi: 10.1083/jcb.115.5.1319.

Liu SC, Derick LH, Palek J. 1987. Visualization of the hexagonal lattice in the erythrocyte membrane skeleton. *The Journal of Cell Biology* **104**:527–536. doi: 10.1083/jcb.104.3.527.

Lorenzo DN, Badea A, Davis J, Hostettler J, He J, Zhong G, Zhuang X, Bennett V. 2014. A PIK3C3-Ankyrin-B-Dynactin pathway promotes axonal growth and multiorganelle transport. *The Journal of Cell Biology* **207**:735–752. doi: 10.1083/jcb.201407063.

Lukinavicius G, Reymond L, D'Este E, Masharina A, Gottfert F, Ta H, Güther A, Fournier M, Rizzo S, Waldmann H, Blaukopf C, Sommer C, Gerlich DW, Arndt HD, Hell SW, Johnsson K. 2014. Fluorogenic probes for live-cell imaging of the cytoskeleton. *Nature Methods* **11**:731–733. doi: 10.1038/nmeth.2972.

Luo L. 2002. Actin cytoskeleton regulation in neuronal morphogenesis and structural plasticity. *Annual Review of Cell and Developmental Biology* **18**:601–635. doi: 10.1146/annurev.cellbio.18.031802.150501.

Pielage J, Cheng L, Fetter RD, Carlton PM, Sedat JW, Davis GW. 2008. A presynaptic giant ankyrin stabilizes the NMJ through regulation of presynaptic microtubules and transsynaptic cell adhesion. *Neuron* **58**:195–209. doi: 10.1016/j.neuron.2008.02.017.

Pielage J, Fetter RD, Davis GW. 2005. Presynaptic spectrin is essential for synapse stabilization, *Current Biology* **15**:918–928. doi: 10.1016/j.cub.2005.04.030.

Riederer BM, Zagon IS, Goodman SR. 1986. Brain spectrin(240/235) and brain spectrin(240/235E): two distinct spectrin subtypes with different locations within mammalian neural cells. *The Journal of Cell Biology* **102**:2088–2097. doi: 10.1083/jcb.102.6.2088.

Rust MJ, Bates M, Zhuang X. 2006. Sub-diffraction-limit imaging by stochastic optical reconstruction microscopy (STORM). *Nature Methods* **3**:793–795. doi: 10.1038/nmeth929.

Sakaguchi G, Orita S, Naito A, Maeda M, Igarashi H, Sasaki T, Takai Y. 1998. A novel brain-specific isoform of beta spectrin: isolation and its interaction with Munc13. *Biochemical and Biophysical Research Communications* **248**:846–851. doi: 10.1006/bbrc.1998.9067.

Scotland P, Zhou D, Benveniste H, Bennett V. 1998. Nervous system defects of AnkyrinB (-/-) mice suggest functional overlap between the cell adhesion molecule L1 and 440-kD AnkyrinB in premyelinated axons. *The Journal of Cell Biology* **143**:1305–1315. doi: 10.1083/jcb.143.5.1305.

Shim SH, Xia C, Zhong G, Babcock HP, Vaughan JC, Huang B, Wang X, Xu C, Bi GQ, Zhuang X. 2012. Super-resolution fluorescence imaging of organelles in live cells with photoswitchable membrane probes. *Proceedings of the National Academy of Sciences of USA* **109**:13978–13983. doi: 10.1073/pnas.1201882109.

Stankewich MC, Cianci CD, Stabach PR, Ji L, Nath A, Morrow JS. 2011. Cell organization, growth, and neural and cardiac development require alphaII-spectrin. *Journal of Cell Science* **124**:3956–3966. doi: 10.1242/jcs.080374.

Stankewich MC, Tse WT, Peters LL, Ch'ng Y, John KM, Stabach PR, Devarajan P, Morrow JS, Lux SE. 1998. A widely expressed betaIII spectrin associated with Golgi and cytoplasmic vesicles. *Proceedings of the National Academy of Sciences of USA* **95**:14158–14163. doi: 10.1073/pnas.95.24.14158.

Stiess M, Bradke F. 2011. Neuronal polarization: the cytoskeleton leads the way. *Developmental Neurobiology* **71**:430–444. doi: 10.1002/Dneu.20849.

Susuki K, Raphael AR, Ogawa Y, Stankewich MC, Peles E, Talbot WS, Rasband MN. 2011. Schwann cell spectrins modulate peripheral nerve myelination. *Proceedings of the National Academy of Sciences of USA* **108**: 8009–8014. doi: 10.1073/pnas.1019600108.

Susuki K, Rasband MN. 2008. Spectrin and ankyrin-based cytoskeletons at polarized domains in myelinated axons. *Experimental Biology and Medicine* **233**:394–400. doi: 10.3181/0709-MR-243.

Tang Y, Katuri V, Dillner A, Mishra B, Deng CX, Mishra L. 2003. Disruption of transforming growth factor-beta signaling in ELF beta-spectrin-deficient mice. *Science* **299**:574–577. doi: 10.1126/science.1075994.

Wang S, Moffitt JR, Dempsey GT, Xie XS, Zhuang X. 2014. Characterization and development of photoactivatable fluorescent proteins for single-molecule-based superresolution imaging. *Proceedings of the National Academy of Sciences of USA* **111**:8452–8457. doi: 10.1073/pnas.1406593111.

Witte H, Neukirchen D, Bradke F. 2008. Microtubule stabilization specifies initial neuronal polarization. *The Journal of Cell Biology* **180**:619–632. doi: 10.1083/jcb.200707042.

Writzl K, Primec ZR, Strazisar BG, Osredkar D, Pecaric-Meglic N, Kranjc BS, Nishiyama K, Matsumoto N, Saitsu H. 2012. Early onset West syndrome with severe hypomyelination and coloboma-like optic discs in a girl with SPTAN1 mutation. *Epilepsia* **53**:e106–e110. doi: 10.1111/j.1528-1167.2012.03437.x.

Xu K, Zhong G, Zhuang X. 2013. Actin, spectrin, and associated proteins form a periodic cytoskeletal structure in axons. *Science* **339**:452–456. doi: 10.1126/science.1232251.

Yang Y, Ogawa Y, Hedstrom KL, Rasband MN. 2007. beta IV spectrin is recruited to axon initial segments and nodes of Ranvier by ankyrinG. *Journal of Cell Biology* **176**:509–519. doi: 10.1083/jcb.200610128.

Yoshimura T, Kawano Y, Arimura N, Kawabata S, Kikuchi A, Kaibuchi K. 2005. GSK-3beta regulates phosphorylation of CRMP-2 and neuronal polarity. *Cell* **120**:137–149. doi: 10.1016/j.cell.2004.11.012.

Zhou D, Lambert S, Malen PL, Carpenter S, Boland LM, Bennett V. 1998. AnkyrinG is required for clustering of voltage-gated Na channels at axon initial segments and for normal action potential firing. *The Journal of Cell Biology* **143**:1295–1304. doi: 10.1083/jcb.143.5.1295.